Journal of the European Ceramic Society 22 (2002) 2945–2956

www.elsevier.com/locate/jeurceramsoc

Thermal shock of ground and polished alumina and Al_2O_3/SiC nanocomposites

S. Maensiri, S.G. Roberts*

Department of Materials, University of Oxford, Parks Road, Oxford, OX1 3PH, UK

Received 29 August 2001; received in revised form 29 January 2002; accepted 24 February 2002

Abstract

The thermal shock behaviour of sintered alumina and alumina/SiC nanocomposites with 1, 2.5 and 5 vol.% SiC was studied. The thermal shock testing was carried out by means of quenching into water from high temperatures (ΔT in the range 0–750 °C). Both single shocks and repeated shocks were used. The damage introduced by thermal shock was characterised by degradation of strength in four-point bending and by changes in Young's modulus. The effects of the surface finish of the test specimens (either ground or highly polished surfaces) on the thermal shock resistance were also studied. In both alumina and nanocomposite materials, specimens with ground surfaces showed a better resistance to thermal shocks than specimens with polished surfaces. However, the resistance of the nanocomposite material to single and repeated thermal shocks was no better than that of the pure alumina.

Keywords: Nanocomposites; Grinding; Polishing; Surface damage; Thermal shock resistance; Al_2O_3/SiC

1. Introduction

Alumina/SiC "nanocomposites" have been researched intensively because they have been reported to have significantly improved mechanical properties over the basic alumina.[1–3] Niihara[1] reported the strength of hot-pressed alumina/5 vol.% SiC to be 1050 MPa (compared with 350 MPa for alumina) and fracture toughness to be 4.8 MPa $m^{1/2}$ (compared with 3.5 MPa $m^{1/2}$ for alumina). Although the potential high strength of these materials is widely acknowledged, only strength values up to 800 MPa have been reported by other research groups.[2–7] The absolute and relative strengths of alumina and alumina/SiC nanocomposite appear to depend strongly on surface quality,[8] with some reports that strengths are identical for well-polished specimens.[9,10] Improvements over monolithic alumina in erosive wear resistance, polishing behaviour and surface quality after grinding and polishing have also been reported.[11,12] However, so far there is no consensus on the mechanism(s) by which the SiC additions improve properties: the so-called "nanocomposite effects".

Recently, Maensiri and Roberts[10] used indentation techniques to study aspects of the thermal shock resistance of sintered alumina/SiC nanocomposites. They found that the nanocomposites with an addition of SiC nanophase as low as 1vol.% have a "surface damage" thermal shock resistance superior to that of pure alumina. However, the mechanisms by which the SiC additions lead to the improvements in thermal shock resistance were still unclear.

In this study, we investigated the thermal shock behaviour of sintered alumina and alumina/SiC nanocomposites using water-quench experiments. The damage introduced by single and repeated thermal shocks was characterised by degradation of strength in four-point bending and by changes in Young's modulus. The effects of the surface finish of the test specimens (either ground or highly polished surfaces) on thermal shock resistance were also investigated.

2. Experimental procedure

2.1. Material preparation and properties

The materials used in this study were pressureless-sintered alumina and alumina with an incorporation of l, 2.5 and 5 vol.% SiC. The experimental procedures

* Corresponding author. Tel.: +44-1865-273775; fax: +44-1865-272764.

E-mail address: steve.roberts@materials.ox.ac.uk (S.G. Roberts).

0955-2219/02/$ - see front matter
PII: S0955-2219(02)00052-3

used to manufacture these materials have been described in detail elsewhere,[10,12] and are briefly outlined here. The materials were produced in lots of 100 g as follows. A commercial α-SiC powder of mean particle size ~200 nm (UF 45, Lonza, Germany) was dispersed in 50 ml of distilled water together with 10 drops of a dispersing agent (Dispex A40, Allied Colloids, UK), and then ultrasonically agitated for 25 min. The SiC slurry was then added to α-Al_2O_3 powder of mean particle size ~400 nm (AES 11C, Sumitomo) and attrition milled at 500 rpm for 2 h. The resultant slurry was freeze-dried, and the dried powder was passed through a 150-μm sieve. Green bodies were prepared from the sieved powder by uniaxial pressing in a 36 mm die with an applied pressure of approximately 42 MPa followed by Cold Isostatic Pressing (CIP) at a pressure of ~200 MPa. The compacts were sintered at 1650–1775 °C for 2–2.5 h in a nitrogen atmosphere. All nanocomposite specimens were sintered in a bed of coarse SiC powder in a graphite crucible. Pure alumina was fabricated using the same procedure with a sintering temperature of 1600 °C in a bed of coarse alumina powder in an alumina crucible. The sintering temperatures for alumina and nanocomposites were chosen as the minimum to give near-full density in each case.

Throughout this paper, "C1%" refers to the alumina/1 vol.% SiC nanocomposite sintered at 1650 °C, "C2.5%" refers to the alumina/2.5 vol.% SiC nanocomposite sintered at 1675 °C, and "C5%" refers to the alumina/5 vol.% SiC nanocomposite sintered at 1700 °C. The basic properties of the alumina and nanocomposites used in this study have been reported elsewhere[10] and are summarised in Table 1. Density of the materials was measured by Archimedes' method, elastic moduli by a resonance technique and hardness and fracture toughness by indentation methods. Strength data are from four-point bend tests as described later.

Fig. 1 shows SEM micrographs of polished and thermally etched specimens. Grain size data were derived from such micrographs by a linear intercept method. The C1% (Fig. 1b) and C2.5% (Fig. 1c) microstructures show some evidence of anomalous grain growth (the amount of SiC used being not quite sufficient to pin alumina grain boundaries at the sintering temperatures used), resulting in larger grains with a broad grain size distribution. The alumina and the C5% nanocomposite (Fig. 1a and e) show a narrower distribution of smaller grain sizes. In some regions of the micrographs of all materials there are several light coloured particles, probably zirconia from the wear of milling media and the attritor bucket during milling. Detailed microstructural analysis was not carried out, but other workers[4,7,8] on similarly produced alumina/SiC nanocomposites have found the ~200 nm SiC particles to be present both within alumina grains and on grain boundaries.

2.2. Specimen preparation

Rectangular bar specimens of size ~22×3×2.5 mm were used for all tests. Specimens were cut with the long dimension parallel to the grinding direction. The tensile and compressive faces and the other two sides of each specimen were machined and then ground or fully polished according to the following procedures. Two specimen surface-finish conditions were used in this study: a ground surface, and a fine polished surface. The ground surfaces were produced on a flat-bed grinder (Jones and Shipman 1400L, UK) using the following conditions: resin-bonded diamond wheel of 150-grit size; grinding wheel speed 1240 rpm; table velocity 0.8 m/s, depth of cut 0.125 mm/pass. The polishing process was carried out after grinding using a Kent Mark 3 disc polishing machine (Engis Ltd, UK). The first two polishing steps each removed at least 150 μm of material with diamond grits of 25 and 8 μm grit size. The third and fourth steps each removed about 50 μm using 3 and 1 μm diamond. This procedure was used to remove completely the influence of surface grinding and results in a surface whose properties are determined by the final polishing steps.

2.3. Thermal shock experiments

Thermal shock experiments were performed in a vertical tube furnace in air. Specimens were inserted into the preheated furnace and were held there for 25 min before quenching by dropping into a bath of water (18±2 °C). Tests were carried out at temperature differences, ΔT, between 135 and 670 °C. Repeated thermal shock tests, up

Table 1
Summary of properties of materials investigated

Material	Sintering temperature (°C)	ρ (%)	Grain size (μm)	K_{IC} (MPa $m^{1/2}$)	E (GPa)	ν	σ_f (MPa)	
							G	P
Alumina	1600	99.6 ±0.06	4.10 ±0.94	2.6 ±0.2	382 ±8	0.24	345 ±60	371 ±10
C1%	1650	100.0 ±0.9	6.85 ±2.47	2.3 ±0.2	415 ±5	0.25	285 ±20	369 ±66
C2.5%	1675	98.1 ±1.4	6.66 ±2.48	2.2 ±0.1	403 ±25	0.25	310 ±30	409 ±67
C5%	1700	99.9 ±0.6	2.82 ±0.51	2.6 ±0.1	397 ±2	0.25	373 ±80	417 ±56

K_{IC}, E, and σ_f denote fracture toughness, Young's modulus and fracture strength, respectively. G and P denote 'ground' and 'polished', respectively.

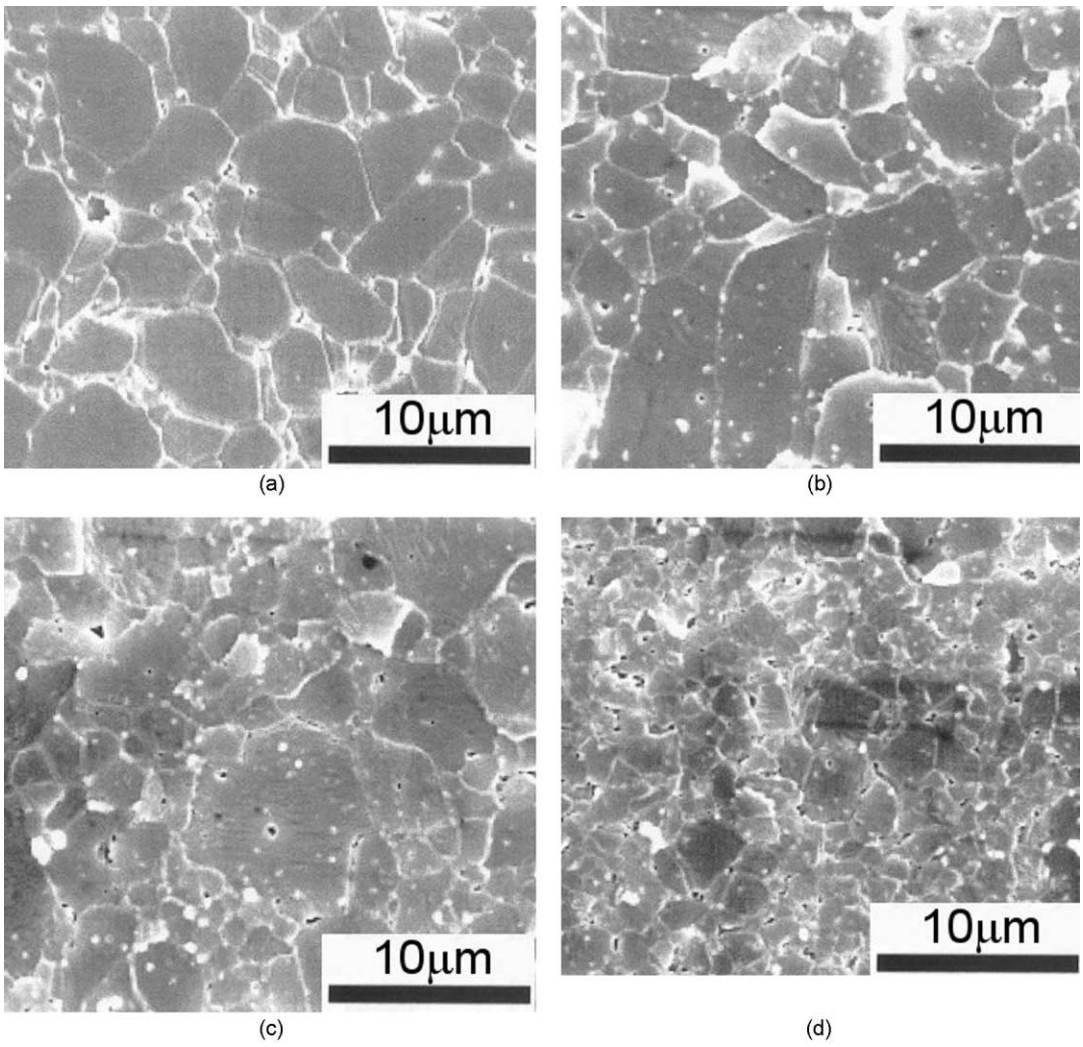

Fig. 1. Microstructures of materials studied: (a) alumina (sintered 1600 °C); (b) Cl%—alumina 1% SiC (sintered 1650 °C); (c) C2.5%—alumina 2.5% SiC (sintered 1675 °C); (d) C5%—alumina 5% SiC (sintered 1700 °C). All specimens thermally etched for 30 min at 1450 °C; SEM secondary electron images.

to 24 cycles, were carried out at $\Delta T = 135$, 200, 235 and 275 °C; specimens were held at the test temperature for 15 min before quenching and then kept cooling in the water bath for 2 min before the next heating/quench cycle.

The fracture strengths of the specimens before and after the water quench were measured using a four-point bend test. The tensile edges were bevelled and then polished with 1-μm diamond to reduce any effects of edge cracks. All tests were carried out on a conventional screw driven loading frame (Instron, model 8561) at a cross-head displacement speed of 0.5 mm/min using a four-point bending rig with an inner span of 6 mm and an outer span of 10 mm. The mean strength and standard deviation for each of the conditions studied was obtained using between three and six specimens.

2.4. Young's modulus measurements

Young's modulus of bar specimens before and after the water quench was measured using an impulse excitation technique (Grindo*Sonic*: Model MK5, J. W. Lemmens, Leuven, Belgium). For single thermal shocks, Young's modulus measurements were made before strength testing. For repeated thermal shock tests, a different set of specimens to those fractured was used for Young' modulus measurements. Mean values and standard deviation for E were obtained using between three and six specimens for each of the conditions studied.

3. Results and discussion

3.1. Surface morphology

Fig. 2 shows micrographs of alumina and nanocomposite surfaces after grinding and polishing. After grinding (Fig. 2a–d), all surfaces show evidence of brittle fracture and plastic flow. The ground surfaces of the alumina and the C1% exhibit severe brittle-fracture damage, whereas the ground surfaces of the C2.5% and

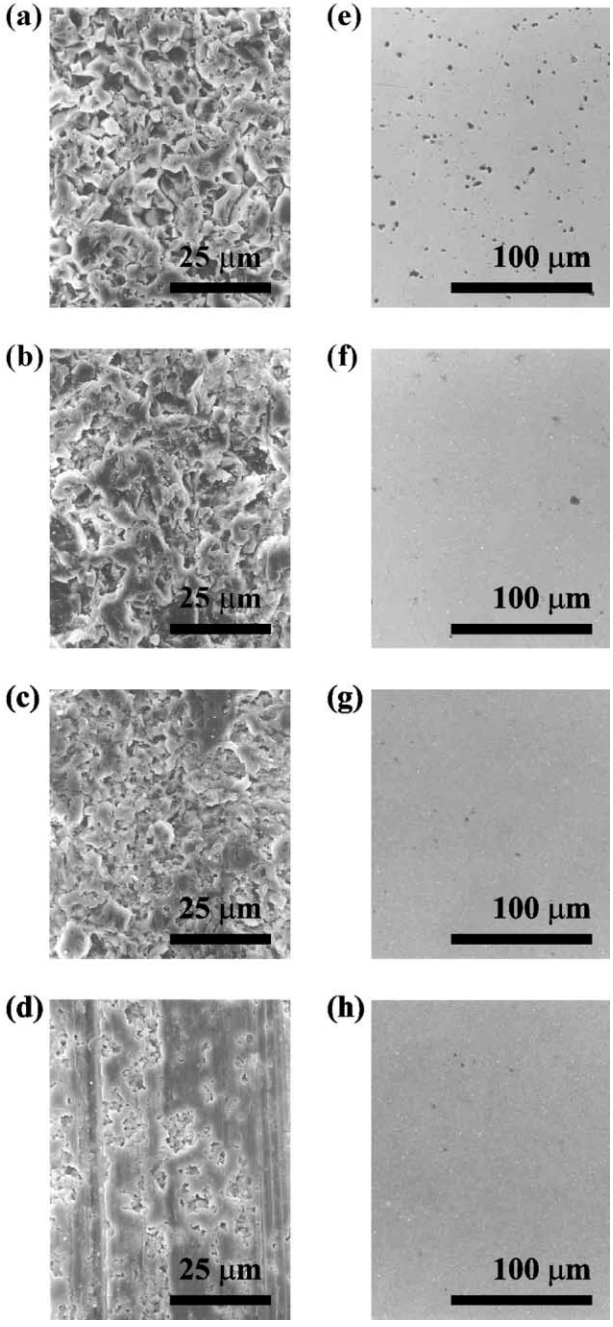

Fig. 2. Surfaces of alumina and nanocomposite specimens after grinding or polishing: (a) and (e) alumina, (b) and (f) C1%, (c) and (g) C2.5%, (d) and (h) C5%. (a–d) are secondary electron images of ground surfaces, (e–h) are optical micrographs of polished surfaces.

C5% specimens show more smooth areas with ploughing scratches running across them indicative of greater plastic flow. The ground alumina surface (Fig. 2a) is dominated by intergranular fracture, and "plastic flow" regions are scarce. The C5% specimen (Fig. 2d) shows a better resistance to grinding damage than the all other materials, though rough patches and holes from local material removal by large-scale fracture can still be seen among the large smooth areas. These observations are consistent with those of Kara and Roberts[12] on ground surfaces of sintered alumina and alumina/SiC nanocomposites and those of Wu et al.[13] on ground hot-pressed alumina and alumina/SiC nanocomposite. The C5% has the finest grain size, and therefore might be expected to show better surface quality. However, the C1% and C2.5%, with bigger grain size than the alumina also show good polished surfaces; also the enhancement of the abrasion resistance of C5% is greater than would be expected from a reduced grain size alone.

For the 1 μm finish (Figs. 2e–h), all the nanocomposites exhibit a better surface finish than that of the pure alumina. No grain pull-out is visible with the nanocomposites, but there are small areas of grain pull-out throughout the alumina surface. These improvements over monolithic alumina in polishing behaviour and surface quality after grinding and polishing of pressureless-sintered Al_2O_3/SiC nanocomposites with SiC volume fraction lower than 5% are again in agreement with the results reported by Kara and Roberts.[12]

The better surface quality of the nanocomposites after grinding and polishing is probably linked to improvements in grain boundary strength, leading to the suppression of intergranular fracture and grain pull-out. Winn and Todd[14] have shown that this behvaviour is linked to the presence of SiC particles on grain boundaries, though the mechanism remains unclear.

3.2. Fracture behaviour of unshocked materials

Four-point bend strengths for all materials are given in Table 1. Note that the fracture toughness values and strengths of the nanocomposites are not significantly higher than those of alumina, in contrast to most earlier findings.[1–7] The appearance of the fracture surfaces, however, were in co-incidence with other reported work, in that the alumina showed nearly completely intergranular fracture, whereas all nanocomposites showed a high degree of transgranular fracture.

3.3. Single thermal shocks

Fig. 3 shows the effect of single thermal shocks on the strength of ground and polished alumina and alumina/SiC nanocomposite specimens. The strength behaviour of all the materials studied follow Hasselman's theory,[15] which predicts a distinct discontinuity with considerable strength degradation at a critical thermal shock temperature difference ΔT_C^{σ}. The experimental values of ΔT_C^{σ} for all materials are summarised in Table 2. The alumina and C5% material have the same ΔT_C^{σ} values for the polished surfaces (185 °C) and for the ground surfaces (235 °C). The ground C1% and C2.5% materials have a marginally lower value of ΔT_C^{σ} of 200 °C. The ΔT_C^{σ} of the alumina in the current study is similar to values reported in the literature.[16–19]

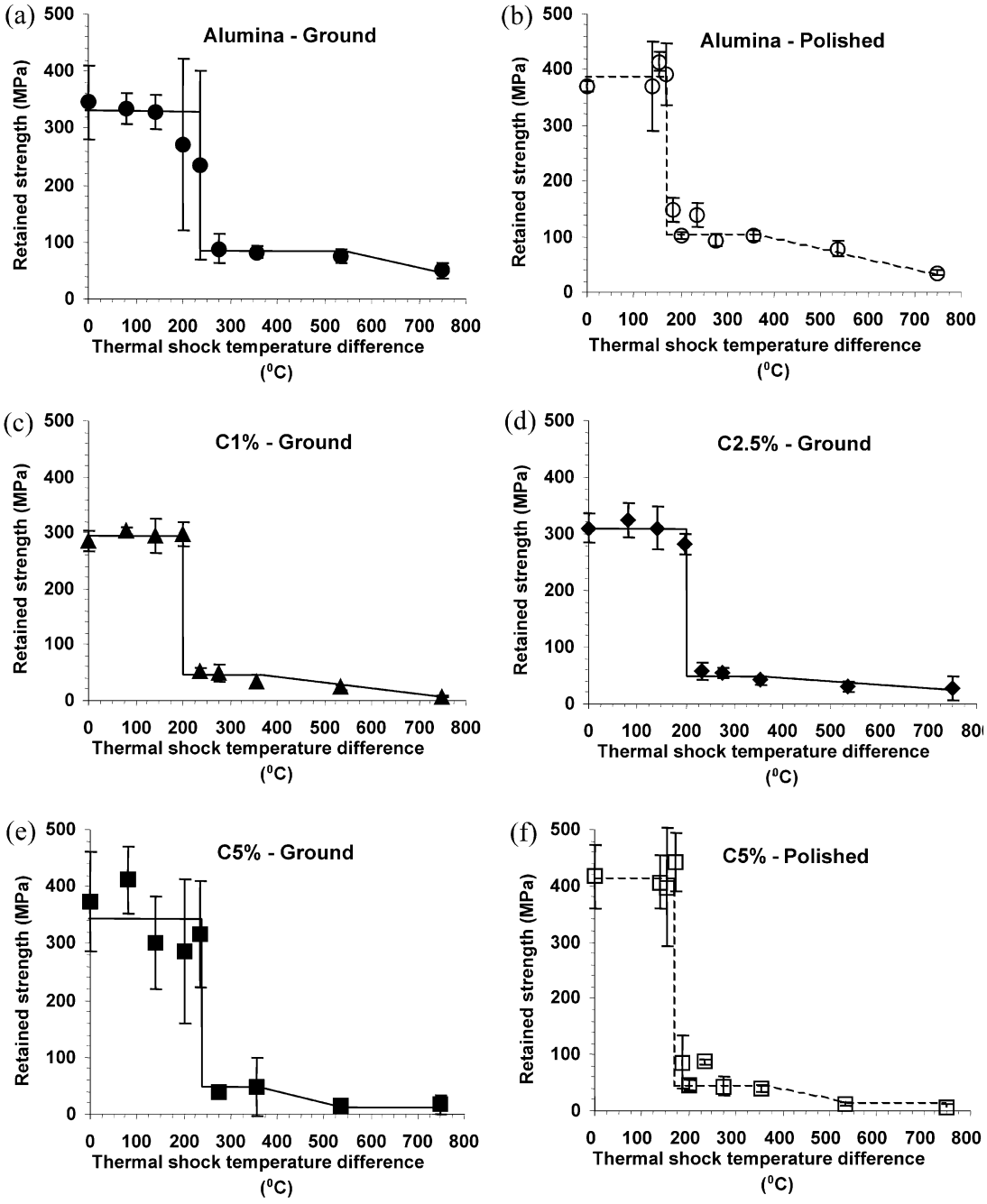

Fig. 3. Retained strength as a function of thermal shock temperature difference (single thermal shock), for alumina and alumina/SiC nanocomposite specimens with ground or polished surfaces.

With further increase in ΔT ($\Delta T > \Delta T_C^{\sigma}$), the strength of the ground and the polished alumina remains constant for a substantial temperature range and then decreases gradually with ΔT up to 750 °C. The strength of the ground and the polished nanocomposites remains constant over a shorter temperature range than for alumina, and then decreases gradually before it becomes constant again. Both ground and polished nanocomposites exhibit lower retained strengths above ΔT_C^{σ} than ground and polished alumina.

The Young's modulus changes as a result of a single thermal shock are shown in Fig. 4. For the ground surfaces, the alumina and C5% material have the same critical thermal shock temperature difference $\Delta T_C^E =$ 235 °C (defined as the temperature difference above which a decrease in Young's modulus begins), and the C1% and the C2.5% materials have the same value of $\Delta T_C^E = 200$ °C. For the polished surfaces, the ΔT_C^E values are respectively 200 °C and 170 °C for the alumina and the C5% material. These ΔT_C^E data are in

Table 2
Thermal shock resistance parameter, R and critical thermal shock temperature differences (ΔT_C^{σ}, ΔT_C^{E} and ΔT_C^{P}) for pressureless-sintered alumina and alumina/SiC nanocomposite

Surface condition	Material	R (°C)	ΔT_C^{σ} (°C)	ΔT_C^{E} (°C)	ΔT_C^{P}, $\beta=5$ (°C)
Ground	Alumina	84	235	235	193
	C1%	69	200	200	158
	C2.5%	76	200	200	175
	C5%	92	235	235	212
Polished	Alumina	90	185	200	207
	C1%	88	–	–	202
	C2.5%	100	–	–	230
	C5%	102	185	170	235

R is defined in Eq. (2). ΔT_C^{σ}: Critical thermal shock temperature difference obtained from strength measurement (σ_f vs ΔT plot). ΔT_C^{E}: critical thermal shock temperature difference obtained from Young's modulus measurement (E vs. ΔT plot). ΔT_C^{P}: critical thermal shock temperature difference predicted using Eq. (1) with $\beta=5$.

good agreement with the ΔT_C^{σ} values from the strength measurements. For $\Delta T > \Delta T_C^{E}$, the Young's modulus of all materials decreases continuously as ΔT increases up to 750 °C; however, ground or polished nanocomposites exhibit a more rapid decrease in Young's modulus than ground or polished alumina. The modulus of the C5% nanocomposite seems to be the most affected by thermal shock damage.

In both the alumina and the nanocomposites, the strength degradation and Young's modulus degradation above ΔT_C were associated with substantial cracking. Fig. 5 shows optical micrographs of thermal-shock-induced surface cracks on well-polished alumina and C5% surfaces. Fig. 5a and b show single cracks propagating from the surface, whereas Fig. 5c shows crack linking. Fig. 6 shows the crack paths of the thermal shock-induced cracks: the fracture type for each material is the same as in bend tests: predominantly intergranular for alumina, transgranular for nanocomposites.

For the thermally shocked ceramic material, it has been proposed[20–24] that a critical thermal shock temperature difference (ΔT_C) can be approximately predicted from the following equations:

$$\Delta T_C^{P} = R\left[1.5 + \frac{A}{\beta} - 0.5\exp\left(-\frac{B}{\beta}\right)\right] = Rf(\beta) \quad (1)$$

$$R = \frac{\sigma_f(1-\nu)}{E\alpha} \quad (2)$$

$$\beta = \frac{th}{k} \quad (3)$$

Here, R is the "instantaneous thermal shock giving fracture" thermal shock parameter, σ_f is the fracture strength, ν is Poisson's ratio, E is Young's modulus,α is the thermal expansion coefficient, β is Biot's modulus, t is a characteristic heat transfer length (half the thickness of the plate), k is thermal conductivity, and h is the surface heat transfer coefficient acting between the plate and the cooling medium. $f(\beta)$ is the damping parameter of the thermal shock (ranging from 0 to 1) and is a function of Biot's modulus. The constants A and B are respectively, 3.25 and 16 for an infinite plate with $0<\beta<20$ [20,21] and are respectively, 4.67 and 51 for a circular rod.[24]

We calculated ΔT_C^{σ} for the materials tested here. Since exact values of A and B are not available for a rectangular bar, it was assumed that A would lie between 3.25 and 4.67 and B would lie between 16 and 51. In this study $A=4$ and $B=30$ were adopted, because a rectangular bar has geometry closer to a rod than to a plate.[24] The materials' properties data were either directly measured (σ_f, ν, E: Table 1) or calculated using standard data[25] together with theoretical models for a particulate composite material (α, k: Table 3). The equations for determining α and k of the composite material are given in the Appendix.

The critical thermal shock temperature differences (ΔT_C^{P}) calculated using Eq. (1) are given in Table 2 for $\beta=5$. According to Eq. (1), predicted ΔT_C values decrease with increasing β, and a polished specimen (high initial strength) is predicted to have a higher ΔT_C than that of a ground specimen (low initial strength). If the results are to be explained by the model underlying Eq. (1), given that α, ν, t and k are roughly temperature-independent and E is constant below ΔT_C, the only remaining variable is the Biot modulus, i.e. the heat transfer co-efficient between quench medium and specimen. However, β values for ground surfaces (Alumina: 2.5; C5%: 3) would then need to be considerably lower than for polished surfaces (e.g. Alumina: 5.5; C5%: 8.6) to fit the experimental data. This seems unlikely.

Alternatively, the improved thermal shock resistance of materials with ground surfaces may be connected with a factor not taken account of in the model leading to Eq. (1): the higher initial flaw density in ground surfaces. The elastic energy made available by thermal shock would be distributed over more cracks, each of

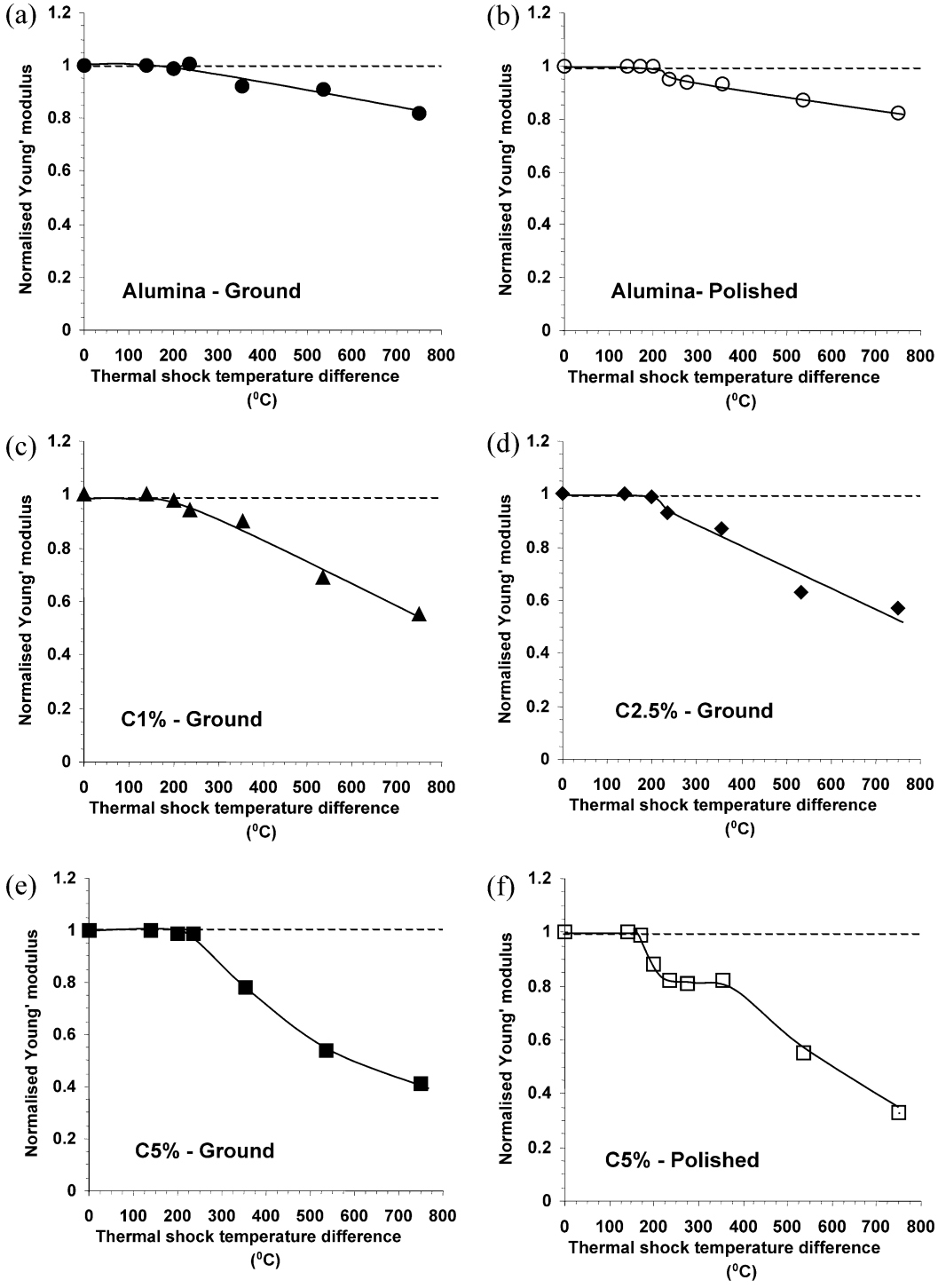

Fig. 4. Young's modulus as a function of thermal shock temperature difference(single thermal shock), for alumina and aluminalSiC nanocomposite specimens with ground or polished surfaces.

which would extend by relatively small amount. On a polished surface, the energy would drive the smaller number of cracks further, leading to considerable strength and modulus reduction. The tendency of the nanocomposite materials to show larger strength degradation than the alumina, especially above ΔT_C, may be as a result of thermal stresses around SiC particles. Under severe thermal shock loading (fast cooling) the thermal expansion mismatch between SiC particles and the matrix alumina will give rise to residual stresses which might cause existing cracks to propagate further in the nanocomposites, or might cause new microcracks to form.

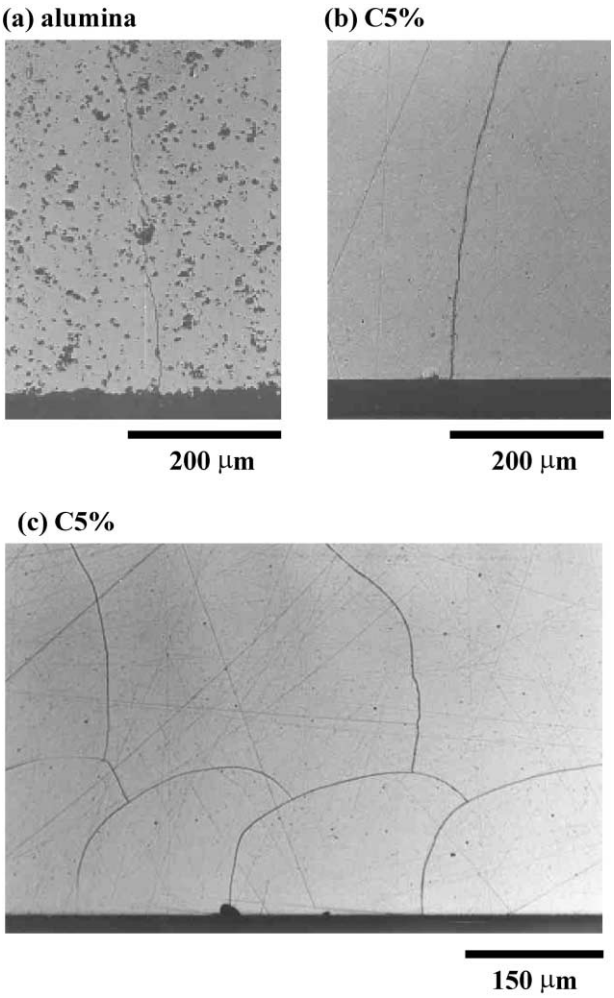

Fig. 5. Optical micrographs showing thermal shock induced surface cracks of well-polished specimens ($\Delta T = 235$ °C). (a) Alumina, (b) and (c) C5%. (a) and (b) show plane strain edge cracking, whereas (c) shows crack linking.

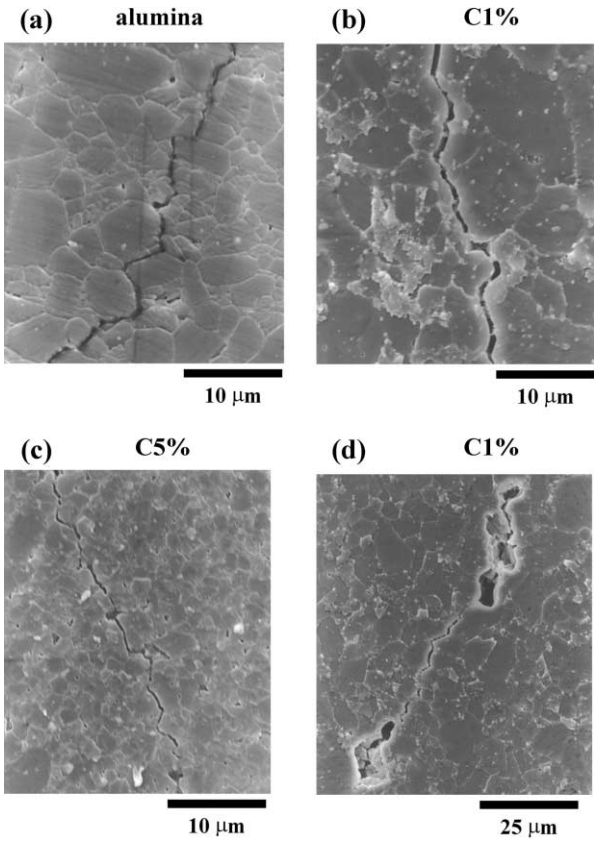

Fig. 6. SEM secondary electron images of thermal-stress fracture cracks in quenched specimens ($\Delta T = 355$ °C). (a) Alumina, showing predominantly intergranular fracture, (b) Cl%, showing transgranular fracture, (c) C5%, showing transgranular fracture and (d) C1%, showing transgranular fracture associated with grain pull out.

3.4. Repeated thermal shocks

Fig. 7 shows the strength of alumina and nanocomposites as a function of the cumulative number of thermal shock cycles quenched at ΔT values of 140, 200, 235 and 275 °C. No significant strength degradation was seen when the materials were repeatedly shocked at $\Delta T = 140$ °C (Fig. 7a; i.e. below ΔT_C). However, at higher ΔT values (i.e. 200, 235 and 275 °C), the strength of all the materials decreased initially rapidly, then tending to saturation values with increasing number of thermal shock cycles. The polished specimens show a rapid drop in strength and then saturate after even a single thermal shock (see Fig. 7b). Repeated thermal shock (RTS) damage was also examined for $\Delta T = 200$ °C by Young's modulus measurement as shown in Fig. 8. These Young's modulus measurements follow the same pattern of behaviour as the results for strength degradation at $\Delta T = 200$ °C shown in Fig. 7b.

Table 3
Thermal properties of all materials investigated (at 25 °C)

Material	Thermal expansion coefficient, α (°C^{-1})	Thermal conductivity, k (Wm^{-1} °C^{-1})
SiC[a]	4.60×10^{-6}	110.0
Alumina[b]	8.00×10^{-6}	38.0
C1%[b]	7.97×10^{-6}	38.4
C2.5%[b]	7.92×10^{-6}	39.1
C5%[b]	7.85×10^{-6}	40.3

[a] Data from Ref. 25
[b] Predicted (see Appendix).

The change in strength and Young's modulus as a function of the cumulative number of thermal shock cycles is presumably because of the accumulation and coalescence of thermal-shock-induced microcrack damage. Such damage could be induced by stresses arising from thermal expansion mismatch between the matrix grains, between alumina and SiC particles, thermal expansion anisotropy of the grains, and stresses from macroscopic thermal gradients present during the quenching in water.[26–28] The alumina/SiC thermal expansion mismatch stresses are of course only present

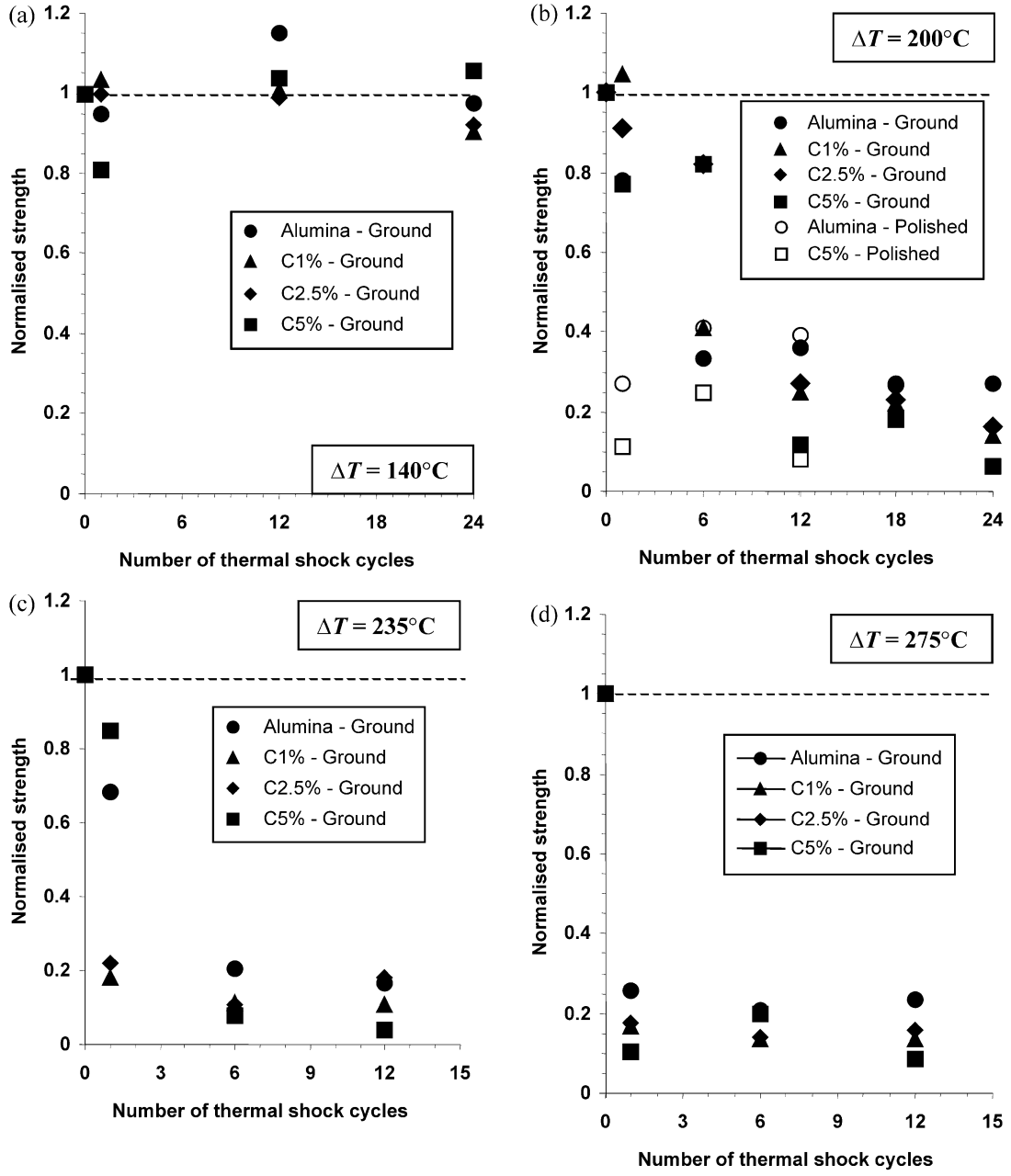

Fig. 7. Effect of repeated thermal shocks on strength of alumina and aluminalSiC nanocomposites. (a) $\Delta T = 140$ °C; (b) $\Delta T = 200$ °C; (c) $\Delta T = 235$ °C; (d) $\Delta T = 275$ °C. Only ground specimens are presented in (a) and (d).

in the nanocomposites, and this may contribute to their lower resistance to thermal shocks, especially as seen in Young's modulus measurements.

The thermal shock damage as measured by both the strength and Young's modulus saturates at a sufficiently high number of thermal shock cycles. Such damage saturation behaviour as a result of repeated thermal shocks has been observed in a number of brittle materials including ceramics and ceramic composites[29–34] and refractories.[35–37] This behaviour can be described using an empirical equation given by Lee and Case[32]:

$$\frac{P}{P_0} = 1 - \frac{D}{P_0}[1 - \exp(-\delta N)] \quad (4)$$

where P is the value of a materials parameter (e.g. σ_f, E, or H) of a specimen subjected to N thermal shocks, P_0 is the value of the parameter for the undamaged state of the specimen, D is the damage saturation level and δ is a rate constant. Eq. (4) implies that higher D and δ are associated with higher levels of thermal shock damage.

For $\Delta T = 200$ °C (Fig. 7b), the highest saturation level of strength is observed in the ground alumina

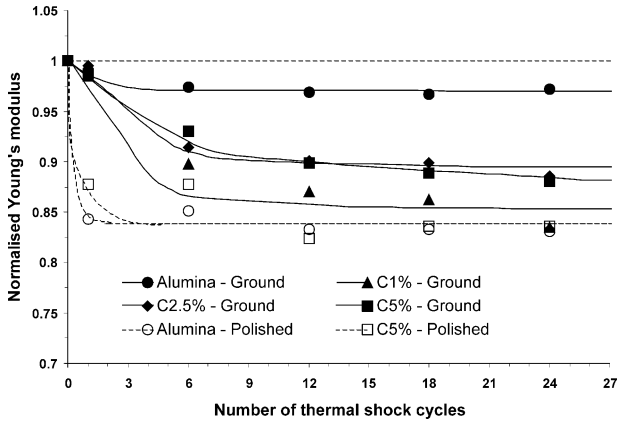

Fig. 8. Effect of repeated thermal shocks on Young's modulus of alumina and alumina/SiC nanocomposites ($\Delta T = 200$ °C).

($D \approx 0.25 \pm 0.05$) and the lowest saturation level of strength is found in the polished C5% ($D \approx 0.10 \pm 0.05$). There is a sudden drop with a quick saturation in retained strength of the polished alumina and polished C5%. This may be because the quenching temperature ($\Delta T = 200$ °C) is higher than ΔT_C^{σ} (≈ 185 °C) for these materials. For specimens with ground surfaces, the gradual decrease and slow saturation may be because the quenching temperature is less than ΔT_C^{σ}. Again, this may be associated with the elastic energy made available by thermal shock being distributed over more cracks, each of which would extend by a relatively small amount. Conversely, on a polished surface, the available energy would drive the smaller number of cracks further, leading to a rapid decrease in strength.

For alumina and C5% nanocomposite at $\Delta T =$ 200 °C; the ground specimens and the polished specimens of each material exhibit the same damage saturation level after 12 thermal shock cycles. However, the different surface finishes give different saturation levels in Young's modulus. This difference may be because the Young's modulus measurement used here considers an "averaged" contribution of all cracks to the behaviour of the whole specimen, whereas even one large flaw on the specimen can affect the strength. It is possible, especially for polished specimens with a low initial crack density, that the thermal shock may produce a few large flaws and many smaller ones. Subsequent thermal shocks may not extend large cracks significantly (local stresses will have been substantially reduced by the presence of the crack), so strength will not be further reduced, but may extend further the small cracks, thus leading to a continuing reduction in modulus.

Similar results were also found for the ground materials repeatedly shocked at $\Delta T = 235$ °C and $\Delta T =$ 275 °C (Figs. 7c and d, respectively). Increasing ΔT causes more thermal shock damage, as indicated by a lower retained strength of all the materials. The materials could thus be ranked in order of increasing resistance to repeated thermal shocks as follows: alumina, C2.5%, C1% and C5% composites. However, the differences between materials are barely significant. The differences between identical materials with different surface finishes are far greater.

4. Conclusions

The thermal shock resistance of sintered alumina and alumina/SiC nanocomposites was studied using a water-quench technique followed by bend strength and Young's modulus measurements. All nanocomposites show a better surface quality than alumina after grinding and polishing. However, the thermal shock resistance of the nanocomposite materials is not significantly better than that of the pure alumina. In both alumina and nanocomposite materials, specimens with ground surfaces show a better resistance to thermal shocks than specimens with polished surfaces. This may be because the higher initial flaw density in ground surfaces allows the elastic energy made available by thermal shock to be distributed over more cracks, each of which would extend by a relatively small amount. On a polished surface, the same energy would drive the smaller number of cracks further.

There is a progressive decrement in strength and Young's modulus for materials subjected to repeated thermal shocks near ΔT_c. The thermal shock damage as measured by both the strength and Young's modulus saturates at a sufficiently high number of thermal shock cycles (between 2 and 12 cycles). The best resistance to repeated thermal shocks is found in the alumina. The microcracking in the alumina is probably controlled by thermal expansion anisotropy mismatch stresses between matrix grains, while in the nanocomposites, additional stresses around SiC particles may result in higher levels of microcracking and thus a lower resistance to repeated thermal shocks.

Acknowledgements

S. Maensiri thanks the Ministry of Science, Technology, and Environment (MSTE), The Royal Thai Government, and Khon Kaen University, Thailand for financial support.

Appendix. Equations for calculations of thermal properties of a particulate composite

Thermal expansion coefficient of a particulate composite (α_c), based on a composite sphere model is given by[38]:

$$\alpha_C = \alpha_m - \left[\frac{3(\alpha_m - \alpha_p)(1-\nu_m)f_p}{\left|(2E_m/E_p)(1-2\nu_p)f_m + 2f_p(1-2\nu_m) + (1+\nu_m)\right|}\right] \quad \text{(A1)}$$

Thermal conductivity of a particulate composite (k_c) based on Rayleigh–Maxwell's model is expressed by[39,40]:

$$k_C = \frac{k_m\left[2k_m + k_p - 2f_p(k_m - k_p)\right]}{2k_m + k_p + f_p(k_m - k_p)}. \quad \text{(A2)}$$

α is the thermal expansion coefficient, k the thermal conductivity, f the volume fraction, ν Poisson's ratio and E Young's modulus. The subscripts p and m refer to particulate and matrix, respectively.

References

1. Niihara, K., New design concept of structural ceramics. *J. Ceram. Soc. Jpn*., 1991, **99**(10), 974–982.
2. Zhao, J., Stearns, L. C., Harmer, M. P., Chan, H. M., Miller, G. A. and Cook, R. F., Mechanical behaviour of alumina-silicon carbide 'nanocomposites'. *J. Am. Ceram. Soc*., 1993, **76**(2), 503–510.
3. Davidge, R. W., Brook, R. J., Cambier, J., Poorteman, M., Leriche, A., O'Sullivan, D., Hampshire, S. and Kennedy, T., Fabrication, properties and modelling of engineering ceramics reinforced with nanoparticles of silicon carbide. *Br. Ceram. Trans*., 1997, **96**(3), 121–127.
4. Stearns, L. C., Zhao, J. and Harmer, M. P., Processing and microstructure development in Al_2O_3/SiC "nanocomposites". J. Eur. Ceram. Soc., 1992, **10**, 473–477.
5. Anya, C. C. and Roberts, S. G., Indentation fracture toughness and surface flaw analysis of sintered alumina/SiC nanocomposites. *J. Eur. Ceram. Soc*., 1996, **16**, 1107–1114.
6. Anya, C. C. and Roberts, S. G., Pressureless sintering and elastic constants of Al_2O_3/SiC nanocomposites. *J. Eur. Ceram. Soc*., 1997, **17**, 565–573.
7. Jeong, Y. K. and Niihara, K., Microstructure and mechanical properties of pressureless sintered Al_2O_3/SiC nanocomposites. *Nanostruct. Mater*., 1997, **9**, 193–196.
8. Wu, H. Z., Lawrence, C. W., Roberts, S. G. and Derby, B., The strength of Al_2O_3/SiC nanocomposites after grinding and annealing. *Acta Mater*., 1998, **46**(11), 3839–3848.
9. Kara, H., *Polishing and Erosive Wear of Pressureless Sintered Low-SiC Alumina/SiC Nanocomposites*. DPhil Thesis, The University of Oxford, Oxford, UK, 2000.
10. Maensiri, S. and Roberts, S.G. Thermal shock behaviour of sintered alumina/SiC nanocomposite evaluated by indentation techniques. *J. Am. Ceram. Soc*. (in press).
11. Kara, H. and Roberts, S.G. Wet erosion of low SiC alumina-SiC nanocomposites, *J. Mat. Sci*. (in press).
12. Kara, H. and Roberts, S. G., Polishing behaviour and surface quality of alumina and alumina/silicon carbide nanocomposites. *J. Am. Ceram. Soc*., 2000, **83**(5), 1219–1225.
13. Wu, H. Z., Roberts, S. G., Winn, A. J. and Derby, B., Residual stress and subsurface damage in alumina and alumina/silicon carbide nanocomposites ceramics. *Acta Mater*., 2001, **49**, 507–517.
14. Winn, A. J. and Todd, R. I., Microstructural requirements for alumina–SiC nanocomposites. *Br. Ceram. Trans*., 1999, **98**(5), 219–224.
15. Hasselman, D. P. H., Unified theory of thermal shock fracture initiation and crack propagation in brittle ceramics. *J. Am. Ceram. Soc*., 1969, **52**, 600–604.
16. Davidge, R. W. and Tappin, G., Thermal shock and fracture in ceramics. *Trans. Brit. Ceram. Soc*., 1967, **66**(8), 405–422.
17. Hasselman, D. P. H., Strength behaviour of polycrystalline alumina subjected to thermal shock. *J. Am. Ceram. Soc*., 1970, **53**(9), 490–495.
18. Gupta, T. K., Strength degradation and crack propagation in thermally shocked Al_2O_3. *J. Am. Ceram. Soc*., 55(5), 249–253.
19. Tomaszewski, H., Influence of microstructure on the thermomechanical properties of alumina ceramics. *Ceram. Int*., 1992, **18**, 51–55.
20. Buessem, W., *Ring Test and Its Application to Thermal Shock Problems. O. A. R. Report*. Wright-Patterson Air Force Base, Dayton, OH, 1950.
21. Manson, S.S. *Behaviour of Materials Under Conditions of Thermal Stress*. N.C.A. Technical Note 2933, Washington DC, 1953.
22. Kingery, D. W., Factors effecting thermal stress resistance of ceramic materials. *J. Am. Ceram. Soc*., 1955, **38**(1), 3–15.
23. Glenny, E. and Royston, M. G., Transient thermal stresses promoted by rapid heating and cooling of brittle circular cylinders. *Trans. Brit. Ceram. Soc*., 1958, **57**, 645–677.
24. Becher, P. F., Lewis III., D., Carman, K. R. and Gonzalez, A. C., Thermal shock resistance of ceramics: size and geometry effects in quench tests. *Am. Ceram. Soc. Bull*., 1980, **59**(5), 542–545.
25. Morrell, R., *Handbook of Properties of Technical & Engineering Ceramics. Part.1; An Introduction for the Engineer and Designer*. The Stationery Office, London, 1985.
26. Lewis III,D., Thermal shock and thermal fatigue testing of ceramics with the water quench test. In *Fracture Mechanics of Ceramics*, Vol. 6, eds. R. C. Bradt, A. G. Evans, D. P. H. Hasselman and F. F. Lange. Plenum Press, New York, 1983, pp. 487–496.
27. Lewis III, D. and Rice, R. W., Thermal shock fatigue of monolithic ceramics and ceramics–ceramic particulate composites. *Ceram. Eng. Sci. Proc*., 1981, **2**(7–8), 712–718.
28. Lewis III, D. and Rice, R. W., Comparison of static, cyclic, and thermal shock fatigue in ceramic composites. *Ceram. Eng. Sci. Proc*., 1982, **3**(9–10), 714–721.
29. Lee, W. J. and Case, E. D., Cyclic thermal shock in SiC-whisker-reinforced alumina composite. *Mater. Sci. Eng*., 1989, **A119**, 113–126.
30. Lee, W. J. and Case, E. D., Thermal fatigue in polycrystalline alumina. *J. Mater. Sci*., 1990, **25**, 5043–5054.
31. Kim, Y., Lee, W. J. and Case, E. D., Thermal fatigue in SiC fiber reinforced aluminosilicate glass-ceramic composite. In *Metal & Ceramic Matrix Composites: Processing, Modelling & Mechanical Behaviour*, ed. R. B. Bhagat, A. H. Clauer, P. Kumar and A. M. Ritter. The Minerals, Metals & Materials Society, Dordrecht, 1990, pp. 479–486.
32. Lee, W. J. and Case, E. D., Comparison of saturation behaviour of thermal shock damage in a variety of brittle materials. *Mater. Sci. Eng*., 1992, **A154**, 1–9.
33. Case, E. D., Kim, Y. and Lee, W. J., Thermal fatigue of ceramics and ceramic composites, eds. T. S. Reinhart and F. H. Froes. In *The Proceedings of the 24th International SAMPE Technical Conference*, Toronto, Canada. Society for the Advancement of Material and Process Engineering, Covina, California, 1992, pp. T1123–T1136.
34. Case, E. D., Kim, Y. and Lee, W. J., Thermal shock in SiC whisker reinforced alumina and in other ceramic systems. In *Thermal Shock and Thermal Fatigue Behaviour of Advanced Ceramics*, ed. G. A. Schneider and G. Petzow. Kluwer Academic Publishers, Dordrecht, 1993, pp. 393–406.
35. Ainsworth, J. H. and Herron, R. H., Thermal shock damage resistance of refractories. *Am. Ceram. Soc. Bull*., 1974, **53**(7), 533–538.
36. Semler, C. E. and Hawisher, T. H., Evaluation of the thermal shock resistance of refractories using the ribbon test method. *Am. Ceram. Soc. Bull*., 1980, **59**, 732–738.

37. Sheu, S. and Scrutton, R., Quenching, polishing, and grinding reaction-bonded silicon nitride. *Am. Ceram. Soc. Bull.*, 1990, **69**(7), 1148–1151.
38. Fahmy, A. A. and Ragai, A. N., Thermal expansion of two-phase solids. *J. Appl. Phys.*, 1970, **41**(13), 5108–5111.
39. Rayleigh, L., On the influence of obstacles arranged in rectangular order upon the properties of a medium. *Phil. Mag.*, 1892, **34**, 481–502.
40. Maxwell, J. C., *A Treatise on Electricity and Magnetism,* Vol. 1, 3rd edn. Oxford University Press, Oxford, 1904.